INTERNATIONAL JOURNAL FOR NUMERICAL METHODS IN FLUIDS
Int. J. Numer. Meth. Fluids 2002; **40**:619–638 (DOI: 10.1002/fld.364)

Highly accurate solutions of the bifurcation structure of mixed-convection heat transfer using spectral method

M. Selmi[1] and K. Nandakumar[2,*,†]

[1]*Department of Mechanical Engineering, University of Qatar, P.O. Box 2713, Doha, Qatar*
[2]*Department of Chemical and Materials Engineering, University of Alberta, Edmonton, Canada T6G 2G6*

SUMMARY

This paper is concerned with producing highly accurate solution and bifurcation structure using the *pseudo-spectral method* for the two-dimensional pressure-driven flow through a horizontal duct of a square cross-section that is heated by a uniform flux in the axial direction with a uniform temperature on the periphery. Two approaches are presented. In one approach, the streamwise vorticity, streamwise momentum and energy equations are solved for the stream function, axial velocity, and temperature. In the second approach, the streamwise vorticity and a combination of the energy and momentum equations are solved for stream function and temperature only. While the second approach solves less number of equations than the first approach, a grid sensitivity analysis has shown no distinct advantage of one method over the other. The overall solution structure composed of two symmetric and four asymmetric branches in the range of Grashof number (Gr) of $0–2 \times 10^6$ for a Prandtl number (Pr) of 0.73 has been computed using the first approach. The computed structure is comparable to that found by Nandakumar and Weinitschke (1991) using a finite difference scheme for Grashof numbers in the range of $0–1 \times 10^6$. The stability properties of some solution branches; however, are different. In particular, the two-cell structure of the isolated symmetric branch that has been found to be unstable by the study of Nandakumar and Weinitschke is found to be stable by the current study. Copyright © 2002 John Wiley & Sons, Ltd.

KEY WORDS: mixed convection; heat transfer; bifurcation phenomena; spectral method

INTRODUCTION

Mixed-convection heat transfer in horizontal ducts is of great importance in the design of heat exchangers and has been studied extensively. There has been sustained improvement in the use of perturbation methods to uncover the solution behaviour and these include works by Morton [1], Iqbal and Stachiewicz [2], Faris and Viskanta [3], and most recently Van Dyke [4]. While perturbation methods are enlighting in certain aspects, they are valid only for small or large values of the dynamical parameter of the problem and cannot deal with

*Correspondence to: K. Nandakumar, Department of Chemical and Materials Engineering, University of Alberta, Edmonton, Canada T6G 2G6.
†E-mail: kumar.nandakumar@ualberta.ca

Received July 1999
Revised February 2002

multiple solutions. Numerical methods are capable of dealing with the problem for adequate range of the dynamical parameter and if equipped with the tools of bifurcation techniques become very powerful in solving for multiple solutions. Earliest investigation of this problem using finite difference techniques (without the use of bifurcation algorithms) was by Cheng and Hwang [5]. Their studies were; however, limited to a Grashof number of 50 000 and only two-cell pattern was observed. Patankar *et al.* [6] examined the case of non-uniform heating and have shown an evidence of transition to a four-cell structure, although no multiple solutions were discovered. Chou and Hwang [7] observed a similar transition for rectangular ducts with uniform heating. The most comprehensive study to date is due to Nandakumar and Weinitschke [8] who have used finite difference techniques and bifurcation techniques to discover as many as five solution branches for a Grashof number up to 10^6. Three of the solution branches exhibit symmetry with respect to the vertical axis, the remaining solution branches are asymmetric. The study revealed that the two-cell structure of the isolated symmetric branch discovered above a Grashof number of about 470 000 was unstable. However, in different studies by Nandakumar *et al.* [9] and by Selmi *et al.* [10] about rotating ducts and rotating curved ducts which exhibit similar bifurcation structure with the current problem, the two-cell flow of the isolated branch was found to be stable. This has prompted us to reexamine the problem by spectral methods, which are known to be more accurate than finite difference methods. We also explore an alternate equivalent formulation that reduces the number of equations to be solved, thus improving the computational efficiency. Thus, the main thrust of the present work is to demonstrate the power, accuracy and efficiency of spectral methods in solving bifurcation problems arising in fluid mechanics.

GOVERNING EQUATIONS

We consider the flow of an incompressible fluid of density ρ and viscosity μ through a rectangular duct of width $2b$ and height $2a$. The position of the duct is horizontal with its axis being perpendicular to the gravity vector and its cross-section may be tilted by an angle ϕ with respect to the gravity vector, as shown in Figure 1. The flow is driven by a constant pressure gradient, $\mathrm{d}p'/\mathrm{d}z'$. The duct is heated by a uniform heat flux along its axis so as to invoke an axially uniform bulk temperature gradient, $\mathrm{d}T_\mathrm{b}'/\mathrm{d}z'$. It is further assumed that the wall temperature, T_w' is uniform at a given cross-section of the duct and a fully developed state exist, $\partial T'/\partial z' = \mathrm{d}T_\mathrm{b}'/\mathrm{d}z'$. The density of the fluid is considered constant except in the buoyancy term, **g**, where the density is approximated by the Boussinesq approximation, $\rho = \rho_\mathrm{r}[1 - \beta(T' - T_\mathrm{r}')]$. Here ρ_r and T_r' denote the density and temperature at a reference state, respectively, and β denotes, the coefficient of thermal expansion of the fluid. With the above assumptions a two-dimensional flow, namely, $\mathbf{v}' = (u'(t', x', y'), v'(t', x', y'), w'(t', x', y'))$ is assumed to exist.

The flow is governed by the continuity, momentum, and energy equations. These equations are made dimensionless using the following scales:

$$x = \frac{x'}{b}, \quad y = \frac{y'}{y}, \quad t = \frac{t'}{a^2/v}, \quad u = \frac{u'}{v/a}, \quad v = \frac{v'}{v/b}, \quad w = \frac{w'}{(-\mathrm{d}p'/\mathrm{d}z')(a^2/\rho v)},$$

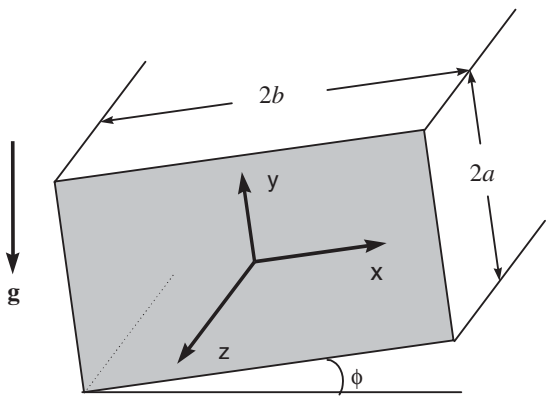

Figure 1. Description of geometry.

$$\theta = \frac{T'_w - T'}{(dT'_b/dz')(-dp'/dz')(a^4/\rho\nu^2)}, \quad p = \frac{p' + \rho g b x' \sin\phi + \rho g a y' \cos\phi}{\rho(\nu^2/a^2)}$$

The normalized governing equations are

$$\frac{\partial u}{\partial x} + \frac{\partial v}{\partial y} = 0 \tag{1}$$

$$\frac{\partial u}{\partial t} + \frac{1}{\gamma}\left(u\frac{\partial u}{\partial x} + v\frac{\partial u}{\partial y}\right) = -\frac{1}{\gamma}\frac{\partial p}{\partial x} + \nabla_\gamma^2 u - \lambda\theta\sin\phi \tag{2}$$

$$\frac{\partial v}{\partial t} + \frac{1}{\gamma}\left(u\frac{\partial v}{\partial x} + v\frac{\partial v}{\partial y}\right) = -\gamma\frac{\partial p}{\partial y} + \nabla_\gamma^2 v - \gamma\lambda\theta\cos\phi \tag{3}$$

$$\frac{\partial w}{\partial t} + \frac{1}{\gamma}\left(u\frac{\partial w}{\partial x} + v\frac{\partial w}{\partial y}\right) = 1 + \nabla_\gamma^2 w \tag{4}$$

$$\frac{\partial \theta}{\partial t} + \frac{1}{\gamma}\left(u\frac{\partial \theta}{\partial x} + v\frac{\partial \theta}{\partial y}\right) - w = \frac{1}{Pr}\nabla_\gamma^2\theta \tag{5}$$

where $\gamma = b/a$ is the aspect ratio, $Pr = \nu/\alpha$ is the Prandtl number and

$$\nabla_\gamma^2 = \frac{1}{\gamma^2}\frac{\partial^2}{\partial x^2} + \frac{\partial^2}{\partial y^2}, \quad \lambda = \frac{g\beta a^7}{\rho\nu^4}\left(\frac{dT'_b}{dz'}\right)\left(-\frac{dp'}{dz'}\right)$$

The stream function ψ is introduced to satisfy the continuity equation implicitly

$$u = \frac{\partial\psi}{\partial y}, \quad v = -\frac{\partial\psi}{\partial x} \tag{6}$$

Taking the curl of the momentum equations produces the vorticity equation having the streamwise component

$$\frac{\partial}{\partial t}(\nabla_\gamma^2\psi)+\frac{1}{\gamma}\left(\frac{\partial\psi}{\partial y}\frac{\partial}{\partial x}(\nabla_\gamma^2\psi)-\frac{\partial\psi}{\partial x}\frac{\partial}{\partial y}(\nabla_\gamma^2\psi)\right)=\lambda\frac{1}{\gamma}\frac{\partial\theta}{\partial x}\cos\phi-\lambda\frac{\partial\theta}{\partial y}\sin\phi+\nabla_\gamma^4\psi \tag{7}$$

and the streamwise momentum and energy equations take the form

$$\frac{\partial w}{\partial t}+\frac{1}{\gamma}\left(\frac{\partial\psi}{\partial y}\frac{\partial w}{\partial x}-\frac{\partial\psi}{\partial x}\frac{\partial w}{\partial y}\right)=1+\nabla_\gamma^2 w \tag{8}$$

$$\frac{\partial\theta}{\partial t}+\frac{1}{\gamma}\left(\frac{\partial\psi}{\partial y}\frac{\partial\theta}{\partial x}-\frac{\partial\psi}{\partial x}\frac{\partial\theta}{\partial y}\right)=w+\frac{1}{Pr}\nabla_\gamma^2\theta \tag{9}$$

Our objective is to solve Equations (7)–(9) for steady-state conditions subject to the no-slip and impermeability conditions at the walls, namely,

$$\psi=\frac{\partial\psi}{\partial x}=w=\theta=0 \quad \text{at } x=\pm 1 \tag{10}$$

$$\psi=\frac{\partial\psi}{\partial y}=w=\theta=0 \quad \text{at } y=\pm 1 \tag{11}$$

Note that the number of equations to be solved has been reduced from 5 to 3. A further reduction to only two equations for ψ and θ is obtained if w from Equation (9) is substituted into Equation. (8) to yield the following equation for steady-state conditions:

$$\begin{aligned}&\frac{1}{\gamma}\frac{\partial\psi}{\partial y}\frac{\partial}{\partial x}\left[\frac{1}{\gamma}\left(\frac{\partial\psi}{\partial y}\frac{\partial\theta}{\partial x}-\frac{\partial\psi}{\partial x}\frac{\partial\theta}{\partial y}\right)-\frac{1}{Pr}\nabla_\gamma^2\theta\right]-\frac{1}{\gamma}\frac{\partial\psi}{\partial x}\frac{\partial}{\partial y}\\&\quad\times\left[\frac{1}{\gamma}\left(\frac{\partial\psi}{\partial y}\frac{\partial\theta}{\partial x}-\frac{\partial\psi}{\partial x}\frac{\partial\theta}{\partial y}\right)-\frac{1}{Pr}\nabla_\gamma^2\theta\right]=1+\nabla_\gamma^2\left[\frac{1}{\gamma}\left(\frac{\partial\psi}{\partial y}\frac{\partial\theta}{\partial x}-\frac{\partial\psi}{\partial x}\frac{\partial\theta}{\partial y}\right)-\frac{1}{Pr}\nabla_\gamma^2\theta\right]\end{aligned} \tag{12}$$

It follows from Equation (5) that the boundary conditions associated with Equation (12) are

$$\theta=\frac{\partial^2\theta}{\partial x^2}=0 \quad \text{at } x=\pm 1 \quad \text{and} \quad \theta=\frac{\partial^2\theta}{\partial y^2}=0 \quad \text{at } y=\pm 1 \tag{13}$$

Numerical method

In this section we present two approaches to solving this problem by the pseudo-spectral method (also known as the spectral collocation method). In the first approach the streamwise vorticity, streamwise momentum, and energy equations (7)–(9) are solved, while in the second approach only the streamwise vorticity equation (7) and the combined energy-momentum equation (12) are solved. For the first approach, the stream function, axial velocity, and

temperature are expanded in Chebyshev series as follows:

$$\psi = \bar{\psi}(x, y) = \sum_{m=0}^{N_x-1} \sum_{n=0}^{N_y-1} C_{mn}^{\psi} F_m^{\psi}(x) G_n^{\psi}(y) \tag{14}$$

$$w = \bar{w}(x, y) = \sum_{m=0}^{N_x-1} \sum_{n=0}^{N_y-1} C_{mn}^{w} F_m^{w}(x) G_n^{w}(y) \tag{15}$$

$$\theta = \bar{\theta}(x, y) = \sum_{m=0}^{N_x-1} \sum_{n=0}^{N_y-1} C_{mn}^{\theta} F_m^{w}(x) G_n^{w}(y) \tag{16}$$

where F_m, G_n are linear combinations of Chebyshev polynomials that satisfy the boundary conditions (10)–(11), namely,

$$F_k^{\psi}(\tilde{x}) = G_k^{\psi}(\tilde{x}) = \alpha_4 T_{l(k+1)+3}(\tilde{x}) + \alpha_2 T_{l(k+1)+1}(\tilde{x}) + \alpha_0 T_{l(k+1)-1}(\tilde{x}) \tag{17}$$

$$F_k^{w}(\tilde{x}) = G_k^{w}(\tilde{x}) = T_{lk+2}(\tilde{x}) - T_{lk}(\tilde{x}) \tag{18}$$

with

$$\alpha_4 = l(k+1), \quad \alpha_2 = -2[l(k+1)+1], \quad \alpha_0 = [l(k+1)+2]$$

for $k = 0, 1, 2, \ldots$, $\tilde{x} \in [-1, 1]$, and l takes the value of 2 if symmetry is enforced and 1 otherwise. Here and only for $\phi = 0$, some of the solution branches are symmetric about the y-axis. Consequently the value of l is set to 2 in the expansion functions in the x-direction, i.e. $l_x = 2$, and is set to 1 in the expansion functions in the y-direction, i.e., $l_y = 1$. That is, in the x-direction, only odd polynomials are included in the expansion functions of the stream function and only even polynomials are included in the expansion functions of the temperature and streamwise velocity. The above series are substituted into Equations (7)–(9) and the resulting equations are satisfied at the collocation points

$$(x_i, y_i) = \left(\cos\left(\frac{(2i+1)\pi}{lN_x} \right), \cos\left(\frac{(2j+1)\pi}{lN_y} \right) \right) \tag{19}$$

This transforms the governing differential equations into a system of $N = 3N_xN_y$ non-linear algebraic equations that may be written in the following form:

$$\mathbf{f}(\mathbf{C}; \chi) = 0 \tag{20}$$

where $\mathbf{f}$ is a vector-valued function and $\mathbf{C}$ is a vector of size N containing the expansion coefficients of the solution and χ is a vector in parameter space, i.e. $\chi = (\gamma, \lambda, Pr, \phi)$.

In the second approach, where Equations (7) and (12) are solved, the expansion series for the stream function stays the same as in the first approach, i.e. Equation (14); however the temperature is expanded as follows:

$$\theta = \bar{\theta}(x, y) = \sum_{m=0}^{N_x-1} \sum_{n=0}^{N_y-1} C_{mn}^{\theta} F_m^{\theta}(x) G_n^{\theta}(y) \tag{21}$$

with

$$F_k^\theta(\tilde{x}) = G_k^\theta(\tilde{x}) = \gamma_4 T_{lk+4}(\tilde{x}) + \gamma_2 T_{lk+2}(\tilde{x}) + \gamma_0 T_{lk}(\tilde{x}) \tag{22}$$

where

$$\gamma_0 = (3 + lk)(19 + 12lk + 2l^2k^2)$$
$$\gamma_2 = -2(2 + lk)(15 + 8lk + 2l^2k^2)$$
$$\gamma_4 = (1 + lk)(3 + 4lk + 2l^2k^2)$$

and similarly when the solution is symmetric with respect to the y-axis, the parameter l in the expansion function in the x-direction is set to 2, otherwise it is set to 1. In the same manner the governing Equations (7) and (12) are collocated at the collocation points (19) to yield a system of non-linear algebraic equations that may be written in the same form as Equation (20).

Equation (20) is solved by Newton–Raphson's iteration

$$\mathbf{C}^i = \mathbf{C}^{i-1} + \delta\mathbf{C}^{i-1} \tag{23}$$

where $\mathbf{C}^i$ denotes the approximate solution vector at the ith iteration, $\mathbf{C}^{i-1}$ denotes the approximate solution vector at the previous or $(i-1)$th iteration and the correction vector $\delta\mathbf{C}^{i-1}$ can be found by solving the linear system

$$J\delta\mathbf{C}^{i-1} = -\mathbf{f}(\mathbf{C}^{i-1}) \tag{24}$$

where J denotes the Jacobian of system (20). Euler's continuation scheme is used to continue solutions along a parameter of interest in parameter space, say λ. If a solution at a specific λ is known, then an approximate solution at $\lambda + \delta\lambda$ can be found through,

$$\mathbf{C}(\lambda + \delta\lambda) = \mathbf{C}(\lambda) + \frac{\partial\mathbf{C}}{\partial\lambda}\,\delta\lambda \tag{25}$$

where $\partial\mathbf{C}/\partial\lambda$ is found from differentiating Equation (20) with respect to λ

$$J\,\frac{\partial\mathbf{C}}{\partial\lambda} = -\,\frac{\partial\mathbf{f}}{\partial\lambda} \tag{26}$$

This requires only one back substitution since J is already factored out during the Newton–Raphson iteration. When this method fails to converge, a nearby singularity is indicated. When this happens we switch to arc-length continuation which requires reparametrizing the problem in terms of the arc-length parameter. Details of how to reparametrize the problem using arc-length is discussed in great details by Selmi *et al.* [10]. Once a solution is obtained, the Grashof number (Gr), mean axial velocity ($\langle w\rangle$), Nusselt number (Nu), and friction factor (f) can be calculated following the definitions given by Nandakumar and Weinitschke [8]

$$\langle w\rangle = \int_{-1}^{1}\int_{-1}^{1} w\,\mathrm{d}x\,\mathrm{d}y/4 \tag{27}$$

$$Gr = 4\lambda\langle w\rangle Pr \tag{28}$$

$$Nu = \frac{4\gamma^2 \langle w \rangle Pr}{(1+\gamma^2)\langle \theta_b \rangle} \tag{29}$$

$$f\,Re = 8\gamma^2/[(1+\gamma^2)\langle w \rangle] \tag{30}$$

where Re is the Reynolds number and θ_b is the average bulk temperature computed as follows:

$$\langle \theta_b \rangle = \int_{-1}^{1} w\theta \, dx \, dy/(4\langle w \rangle) \tag{31}$$

STABILITY ANALYSIS

For convenience, we will only consider the first approach. If a steady-state solution (say $\bar{\psi}$, $\bar{w}$ and $\bar{\theta}$) is found, its stability property is determined by solving for the eigenvalues (σ) resulting from introducing into the governing equations (7)–(9) the time-dependent solution,

$$\psi = \bar{\psi} + \hat{\psi}(x, y)e^{\sigma t} \tag{30}$$

$$w = \bar{w} + \hat{w}(x, y)e^{\sigma t} \tag{31}$$

$$\theta = \bar{\theta} + \hat{\theta}(x, y)e^{\sigma t} \tag{32}$$

where $\hat{\psi}$, $\hat{w}$, and $\hat{\theta}$ are normal modes which are expanded in series of Chebyshev polynomials as in Equations (14)–(16), i.e.

$$\hat{\psi} = \sum_{m=0}^{N_x-1} \sum_{n=0}^{N_y-1} \hat{C}^{\psi}_{mn} F^{\psi}_m(x) G^{\psi}_n(y) \tag{33}$$

$$\hat{w} = \sum_{m=0}^{N_x-1} \sum_{n=0}^{N_y-1} \hat{C}^{w}_{mn} F^{w}_m(x) G^{w}_n(y) \tag{34}$$

$$\hat{\theta} = \sum_{m=0}^{N_x-1} \sum_{n=0}^{N_y-1} \hat{C}^{\theta}_{mn} F^{w}_m(x) G^{w}_n(y) \tag{35}$$

The disturbance modes above can be enforced to be of the symmetric, anti-symmetric, or asymmetric type. For asymmetric solutions, we solve for the asymmetric modes which include both symmetric and anti-symmetric modes and the expansion functions of the solutions and disturbances are the same ($l_x = l_y = 1$). For symmetric solutions, we solve for symmetric disturbances and similarly the expansion functions of the solutions and disturbances are the same ($l_x = 2,\ l_y = 1$). It is also possible for symmetric solutions to solve for anti-symmetric disturbances only. This is possible if the expansion functions in the x-direction for the disturbances are selected such that they are made of odd polynomials for the velocity and temperature and even polynomials for the stream function (opposite to the expansion functions of the solution). For both anti-symmetric and symmetric modes, the normal-mode equations are collocated throughout only half the domain using the collocation points (19), which leads to significant saving in computational power and increases the accuracy of the solution. For all modes the discretized normal-mode equations lead to the generalized eigenvalue problem

$$J\tilde{\mathbf{C}} = \sigma M \tilde{\mathbf{C}} \tag{36}$$

which is solved by an eigenvalue problem solver. It is possible to couple Equations (20) and (36) for zero eigenvalue ($\sigma = 0$) to form an extended system of size $2N$ to solve for critical points such as quadratic limit points and symmetry-breaking bifurcation points. The extended system is also solved by Newton–Raphson iteration and has been discussed in great details by Nandakumar *et al.* [9] and Selmi *et al.* [10].

RESULTS AND DISCUSSION

The pressure-driven flow through a heated duct is known to exhibit multiple solutions. Accurate calculation of these solutions and accurate prediction of their stability properties is quite important in understanding the bifurcation properties of such problem. To date the most comprehensive study about the subject is due to Nandakumar and Weinitschke [8] by using a finite difference scheme. Therefore, throughout this paper comparisons are made with their study to highlight the power of spectral methods against finite difference techniques.

State diagrams representing these solutions are shown in Figure 2 in terms of dimensionless temperature and stream function at ($x = 0.1,\ y = -0.8$) versus λ and in Figure 3 in terms of friction factor and Nusselt number versus Grashof number. Two symmetric (S1, S2) and four asymmetric (AS1–AS4) solution branches have been found for Grashof number up to 2×10^6. The primary branch S1 is computed by starting from a solution at $\lambda = 0$ which corresponds to a forced convection case. Continuation along the positive direction of λ up to $\lambda \sim 1 \times 10^7$ produces the symmetric branch S1 having the two limit points L1 and L2, with two-cell structure before limit point L2 (Figure 4(a)–(c)), a weak four-cell structure in between L1 and L2 (Figure 4(d)–(f), and a strong four-cell structure after L1 (Figure 4(g)–(i)).

A solution on the asymmetric branch AS1 (see Figure 4(j)–(l)) is needed as a starting point for the arc-length continuation scheme to complete the whole branch. One way of finding a starting solution on AS1 is to solve for the solution at the symmetry-breaking point SB1 using the extended system approach discussed in the previous section. Another way of finding a solution on AS1 is to generate an asymmetric branch from $\lambda = 0$ for a small tilt angle, say $\phi = 1^\circ$ and continue the solution branch slightly above limit point L2. One of the solutions on this asymmetric branch slightly above L2 can be used as a first guess for the Newton–Raphson iteration to generate a solution on AS1. Similarly, this procedure can be used to generate the asymmetric branches AS2–AS4. The best way to generate the symmetric branch S2; however, is to solve for the solution at limit point L4 using the solution at SB2 as a first guess. Once the solution at L4 is found, continuation in both directions generates the symmetric branch S2.

Table I presents comparisons between our results (using the first approach) in terms of friction factor and Nusselt number with the results of Nandakumar and Weinitschke [8] for different resolutions at $\lambda = 0$, 25×10^4, and 3×10^6 on the symmetric branch S1. For the case of forced convection ($\lambda = 0$) the comparison is quite good (relative error $\sim 0.06\%$). Also for $\lambda = 0$, our results show four digits of accuracy obtainable with as low as 8×8 polynomials in the x and y direction, respectively. The finite difference results, on the other hand, show only one digit of accuracy. As λ is increased to 25×10^4 and 3×10^6, the relative error has increased to 0.2 and 0.4%, respectively, which is still relatively small. The increase in relative error, however, is due to the fact that as λ increases the physical complexity of the problem increases and consequently it demands higher resolution. We have stretched the resolution

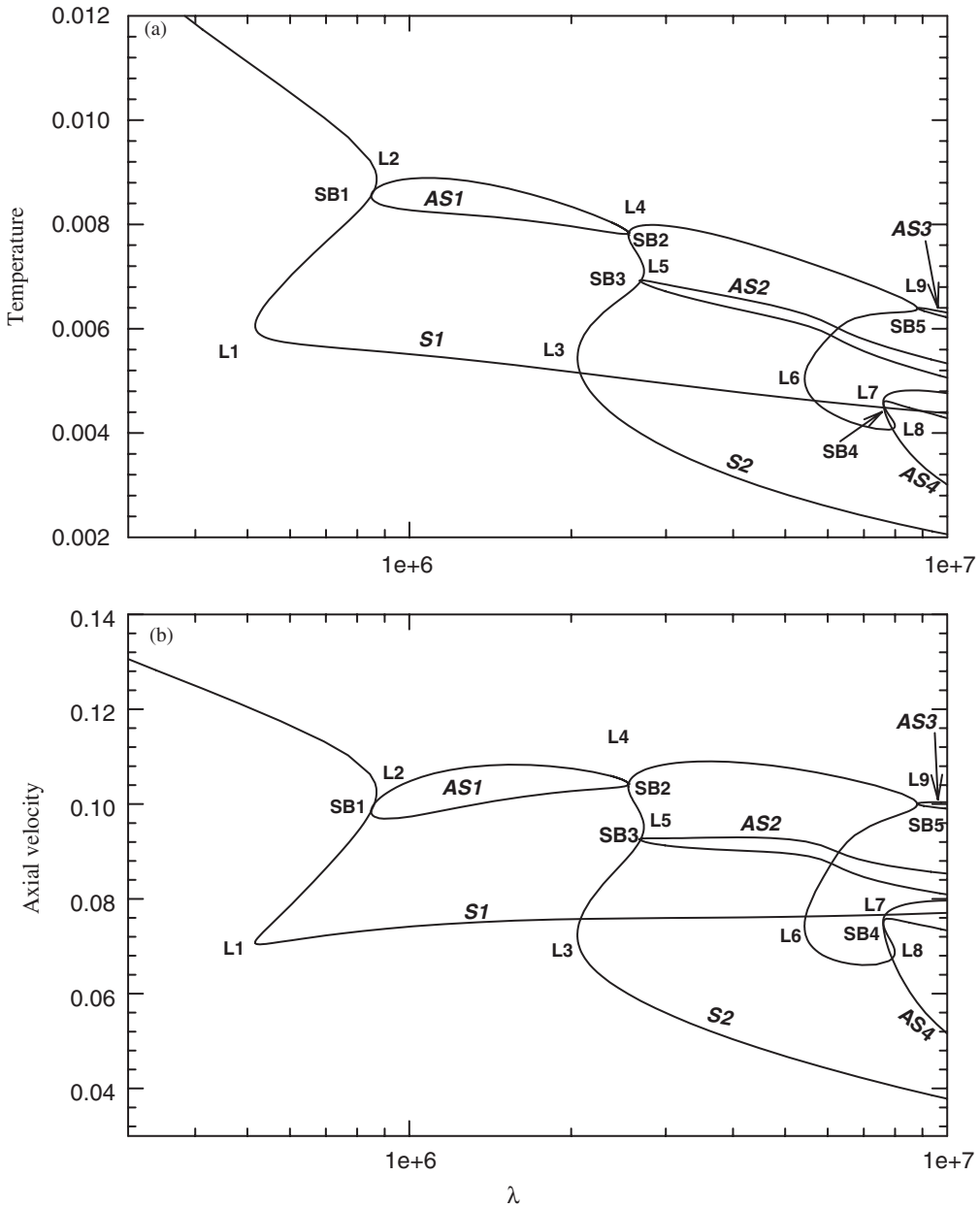

Figure 2. State diagram showing the solution structure for $\gamma = 1$, $\phi = 0$, $Pr = 0.73$: (a) temperature at $(x = 0.1,\ y = -0.8)$ vs λ, (b) stream function at $(x = 0.1,\ y = -0.8)$ vs λ. L1–L9 are limit points. SB1–SB5 are symmetry-breaking bifurcation points.

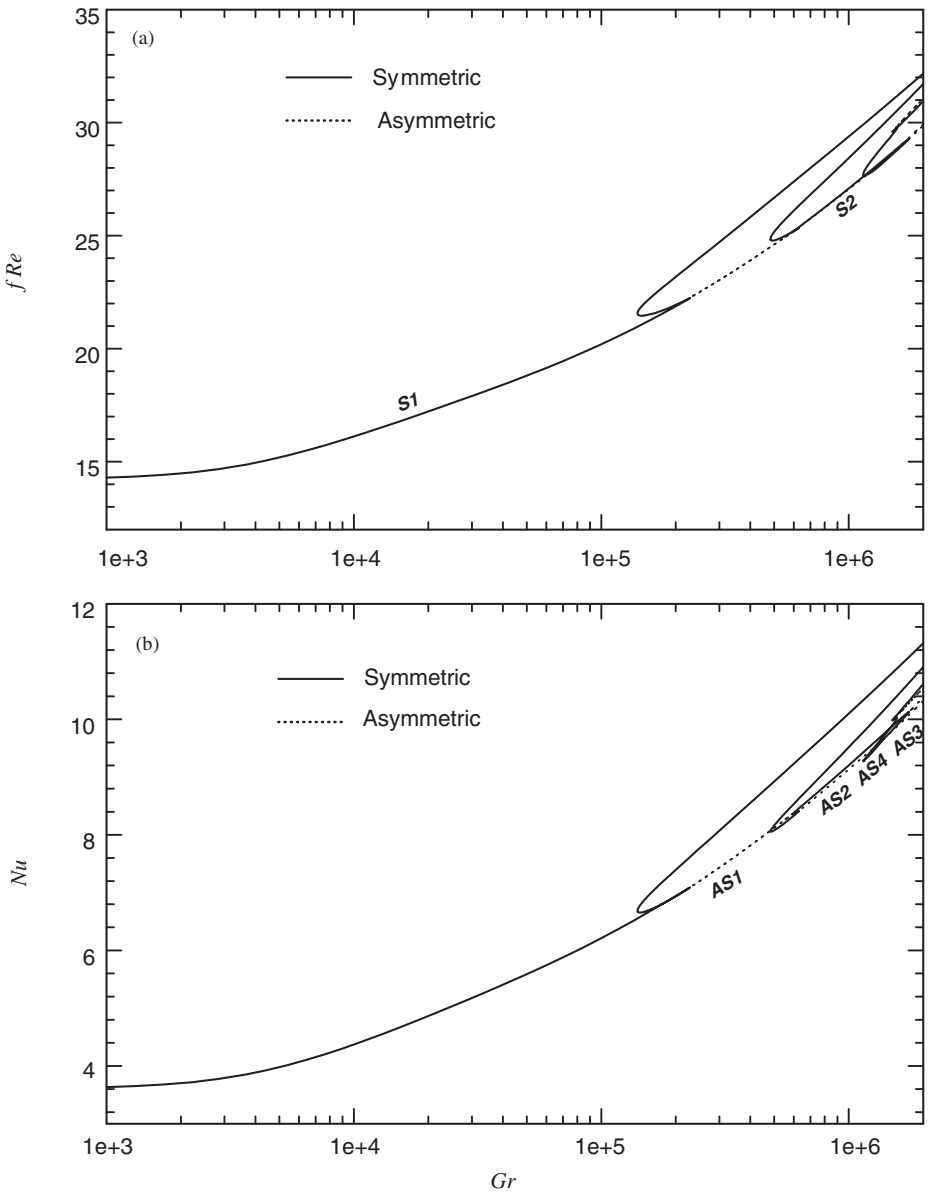

Figure 3. State diagram showing the solution structure for $\gamma = 1$, $\phi = 0$, $Pr = 0.73$: (a) Nu vs Gr, (b) $f\,Re$ vs Gr.

here to 18×18 polynomials and for comparison purposes, the highest reported resolution of 19×39 was taken for the finite difference results.

To further make sure of the convergence of our results and to investigate the difference between our two approaches throughout the parameter range of $\lambda \in [0, 1 \times 10^7]$, we have

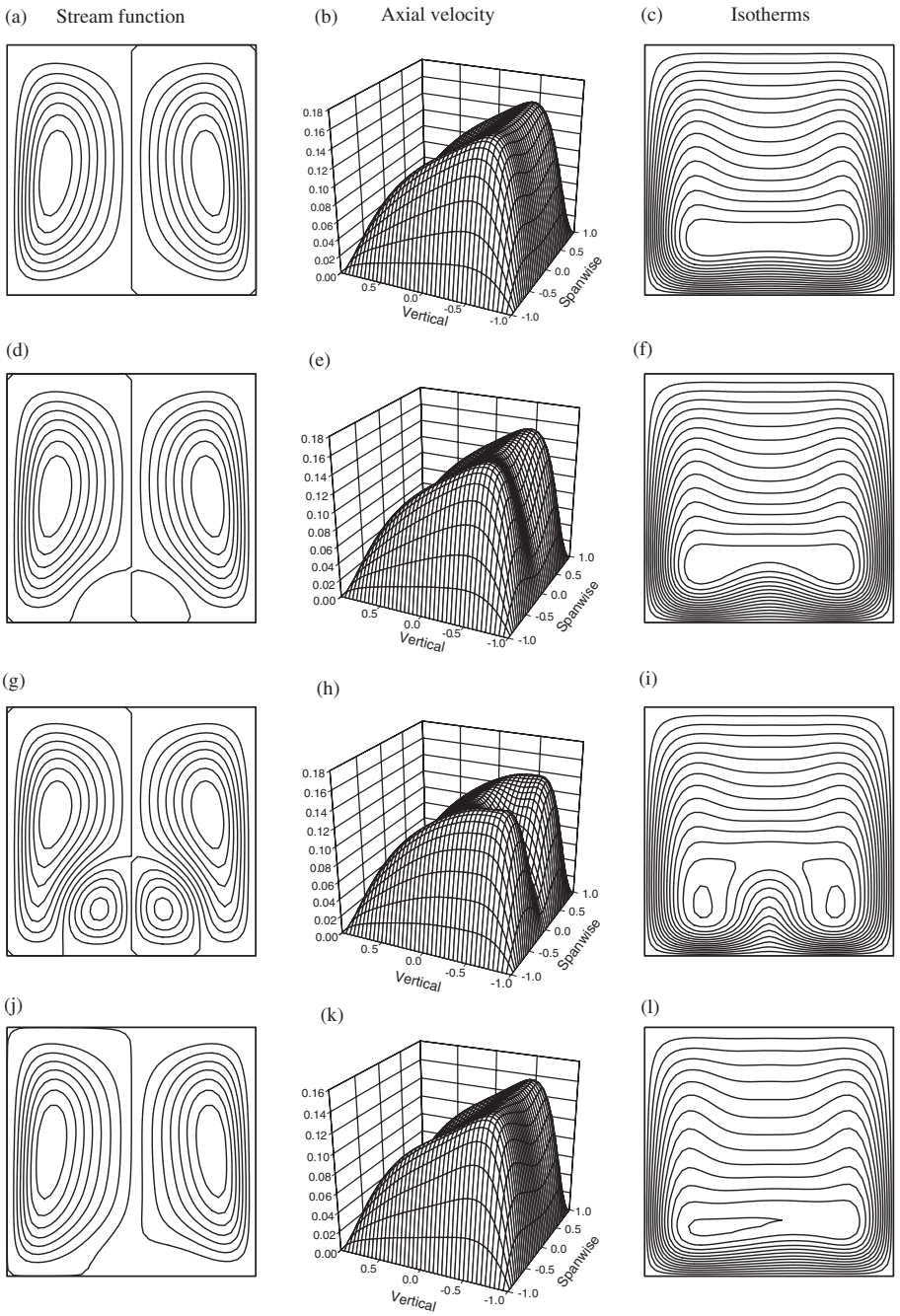

Figure 4. Contour plots for the stream function, axial velocity perspective plots and isotherm contours for $\gamma = 1$, $Pr = 0.73$, $\phi = 0°$. (a–c) solution at $\lambda = 7 \times 10^5$ on S1 before L2, (d–f) solution at $\lambda = 7 \times 10^5$ on S1 between L1 and L2, (g–i) solution at $\lambda = 7 \times 10^5$ on S1 after L2, (j–l) one solution at $\lambda = 1.5 \times 10^6$ on AS1, the second one is a mirror image of this one.

Table I. Grid sensitivity tests using the first approach and comparison at regular points ($\gamma = 1,\ Pr = 0.73,\ \phi = 0^\circ$).

	λ	$N_x \times N_y$	$f\,Re$	Nu
Numerical	0	4×4	14.2368	3.5953
		6×6	14.2272	3.6080
		8×8	14.2271	3.6080
		10×10	14.2271	3.6080
		12×12	14.2271	3.6080
Reference [8]	0	9×19	14.2584	3.5994
		14×29	14.2410	3.6042
		19×39	14.2349	3.6058
Numerical	25×10^4	8×8	19.5822	5.9330
		10×10	19.5739	5.9393
		12×12	19.5767	5.9373
		14×14	19.5766	5.9372
		16×16	19.5767	5.9372
		18×18	19.5767	5.9372
Reference [8]	25×10^6	9×19	19.6916	5.9127
		14×29	19.6134	5.9203
		19×39	19.5931	5.9261
Numerical	3×10^6	8×8	25.4014	8.5338
		10×10	27.2284	9.1807
		12×12	27.6541	9.3096
		14×14	27.6119	9.3299
		16×16	27.5951	9.3250
		18×18	27.6070	9.3262
Reference [8]	3×10^6	9×19	28.2905	9.4243
		14×29	27.8406	9.3324
		19×39	27.7118	9.3171

presented in Figure 5 our results in terms of temperature at a point versus λ for different resolutions employing the two approaches. As can be seen from the figure, relatively low resolution may be adequate for low values of λ, but are not for higher values of λ and near limit points where the solution structure is complicated and demand higher resolution. Also we notice that a lower resolution may be adequate for the first approach while it is not for the second approach. To further explore this point we have shown in Figure 6 the relative error in locating limit point L2 for various resolutions computed by the first and second approaches and also reported by Nandakumar and Weinitschke [9] for the finite difference scheme. The figure clearly shows that while the error for the spectral method drops sharply with the increase in $N_x + N_y$, which is indicative of spectral convergence behaviour, the error for the finite difference scheme drops at a much slower rate as $N_x + N_y$ is increased which is indicative of linear convergence behaviour. For the same error, both approaches of the spectral method require low resolutions compared to the finite difference scheme; however,

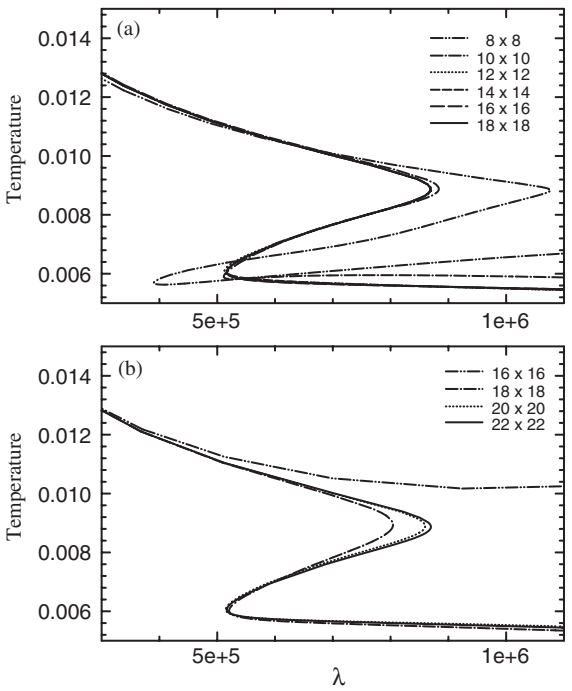

Figure 5. Grid sensitivity test on the symmetric branch S1. Temperature at ($x = 0.1$, $y = -0.8$) vs λ for $\gamma = 1$, $Pr = 0.73$, $\phi = 0^\circ$: (a) first approach, (b) second approach.

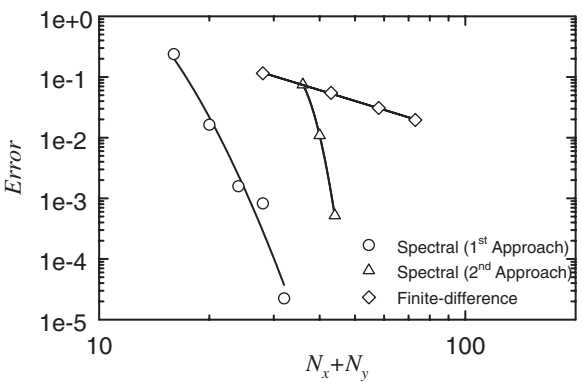

Figure 6. Variation of relative error in terms of λ in locating limit point L1 for $\gamma = 1$, $Pr = 0.73$, $\phi = 0^\circ$.

the second approach requires larger resolution than the first one, and we felt that there is no advantage in terms of savings in computational power for adopting the second approach over the first one even though we are solving fewer number of equations. Consequently, unless otherwise indicated our results are computed by the first approach. We also felt that a resolution of 16×16 is adequate enough for the symmetric solutions to cover the range of λ of

Table II. Grid sensitivity tests for limit points L1 and L2 ($\gamma = 1,\ Pr = 0.73,\ \phi = 0^\circ$).

	Point	$N_x \times N_y$	λ	Gr
Numerical	L1	8×8	390 447	109 460
		10×10	511 435	138 788
		12×12	512 648	139 115
		14×14	516 712	140 088
		16×16	516 878	140 129
		18×18	516 871	140 121
Reference [8]	L1	9×19	517 384	139 226
		14×29	516 737	139 812
		19×39	516 828	140 011
		24×49	516 882	140 082
Numerical	L2	8×8	1 076 292	277 697
		10×10	883 533	231 651
		12×12	870 744	228 604
		14×14	868 657	228 148
		16×16	869 391	228 321
		18×18	869 371	228 316
Reference [8]	L2	9×19	769 238	202 838
		14×29	821 757	216 571
		19×39	842 538	221 806
		24×49	852 366	224 233

our interest. For the asymmetric solutions a resolution of 32×16 was used throughout the study. Table II also presents the locations (in terms of λ and Gr) of limit points L1 and L2 for different resolutions and comparisons with the finite difference results of Nandakumar and Weinitschke [8]. The table shows that a resolution of 16×16 is also quite adequate in predicting limit points L1 and L2, and are within the range of values reported by Nandakumar and Weinitschke (0.002–2% relative error in terms of λ), although our results show better convergence than the finite difference ones.

Limit points and symmetry-breaking bifurcation points are computed using the extended system discussed earlier which in addition to locating the singular point, it solves for the solution and the eigenfunction corresponding to a zero eigenvalue. For limit points both the solution and eigenfunctions are symmetric while for symmetry-breaking bifurcation points the solution is symmetric and the eigenfunctions are anti-symmetric. In any case only half the grid is used and if a solution at a symmetry-breaking bifurcation is already obtained by the extended system it needs to be converted to an asymmetric grid before using it as a starting point to compute an asymmetric branch. Table III presents the computed limit and symmetry-breaking points as well as a comparison with the results of Nandakumar and Weinitschke [8]. The relative error between our results and the finite difference results varies from 0.03% for low Grashof numbers to 10% for high Grashof numbers. At higher Grashof numbers, the relatively significant disagreement is generally attributed to the low resolution of finite difference techniques as compared to spectral methods.

Table III. Computed limit and symmetry-breaking bifurcation points ($\gamma = 1$, $Pr = 0.73$, $\phi = 0°$).

	Point	λ	Gr
Numerical	L1	0.516878×10^6	0.140129×10^6
	SB1	0.849074×10^6	0.223470×10^6
	L2	0.869391×10^6	0.228321×10^6
	L3	0.205423×10^7	0.482983×10^6
	L4	0.255417×10^7	0.592890×10^6
	SB2	0.255749×10^7	0.593528×10^6
	SB3	0.269634×10^7	0.621995×10^6
	L5	0.273023×10^7	0.629006×10^6
	L6	0.543210×10^7	0.114536×10^7
	L7	0.760275×10^7	0.150066×10^7
	SB4	0.761009×10^7	0.150192×10^7
	L8	0.799338×10^7	0.156901×10^7
	SB5	0.879277×10^7	0.175337×10^7
	L9	0.879361×10^6	0.175357×10^7
Reference [8]	L1	0.516738×10^6	0.139812×10^6
	SB1	0.798048×10^6	0.210866×10^6
	L2	0.821757×10^6	0.216571×10^6
	L3	0.200737×10^7	0.471546×10^6
	L4	0.241743×10^7	0.562491×10^6
	SB2	0.242798×10^7	0.562830×10^6
	SB3	0.242798×10^7	0.564569×10^6
	L5	0.245174×10^7	0.569564×10^6

Figures 7 and 8 present some of the solutions in terms of contour plots for stream function, perspective plots for the axial velocity, and contour plots for the isotherms at $\lambda = 7 \times 10^6$ and 1×10^7, respectively, for $\gamma = 1$, $Pr = 0.73$, and $\phi = 0°$. The calculated eigenvalues corresponding to these solutions and those presented in Figure 4 are presented in Table IV. Similar to the results of Nandakumar and Weinitschke [8], the two-cell structure on S1 is stable to both symmetric and anti-symmetric disturbances, the weak four-cell structure on S1 between L1 and L2 is unstable, and the four-cell structure on S1 after L2 is only stable to symmetric disturbances. Although Nandakumar and Weinitschke have reported a change in the stability of S2 at $\lambda = 3 \times 10^6$, we believe this is due to a spurious mode perhaps due to the lack of grid refinement. As for the isolated symmetric branch, our calculations show that the two-cell structure of S2 after L4 is stable contrary to what has been reported by Nandakumar and Weinitschke. All other structures on S2 are unstable to both symmetric and anti-symmetric disturbances, although some of them do not develop as many unstable modes as what has been reported by Nandakumar and Weinitschke. All asymmetric branches have been found to be unstable developing many unstable modes. We believe our results are correct since we have seen this behaviour in other problems such as the flow through rotating ducts investigated by Nandakumar *et al.* [9] and the flow through rotating curved ducts investigated by Selmi *et al.* [10].

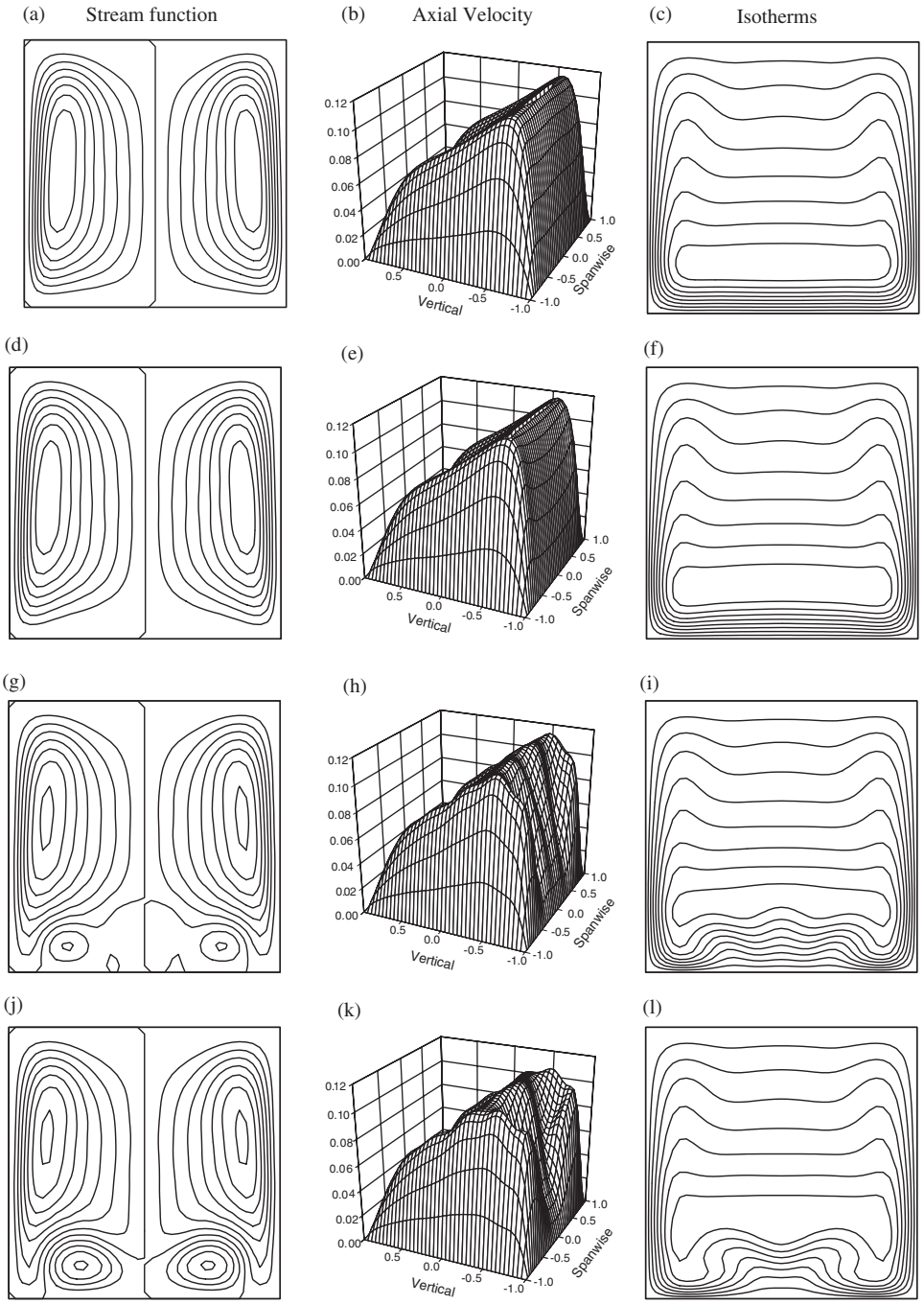

Figure 7. Contour plots for the stream function, axial velocity perspective plots, and isotherm contours for $\lambda = 7 \times 10^6$, $\gamma = 1$, $Pr = 0.73$, $\phi = 0^\circ$. (a–c) solution on S2 between L4 and L9, (d–f) solution on S2 between L6 and L9, (g–i) solution on S2 between L6 and L8, (j–l) solution on S2 after L3.

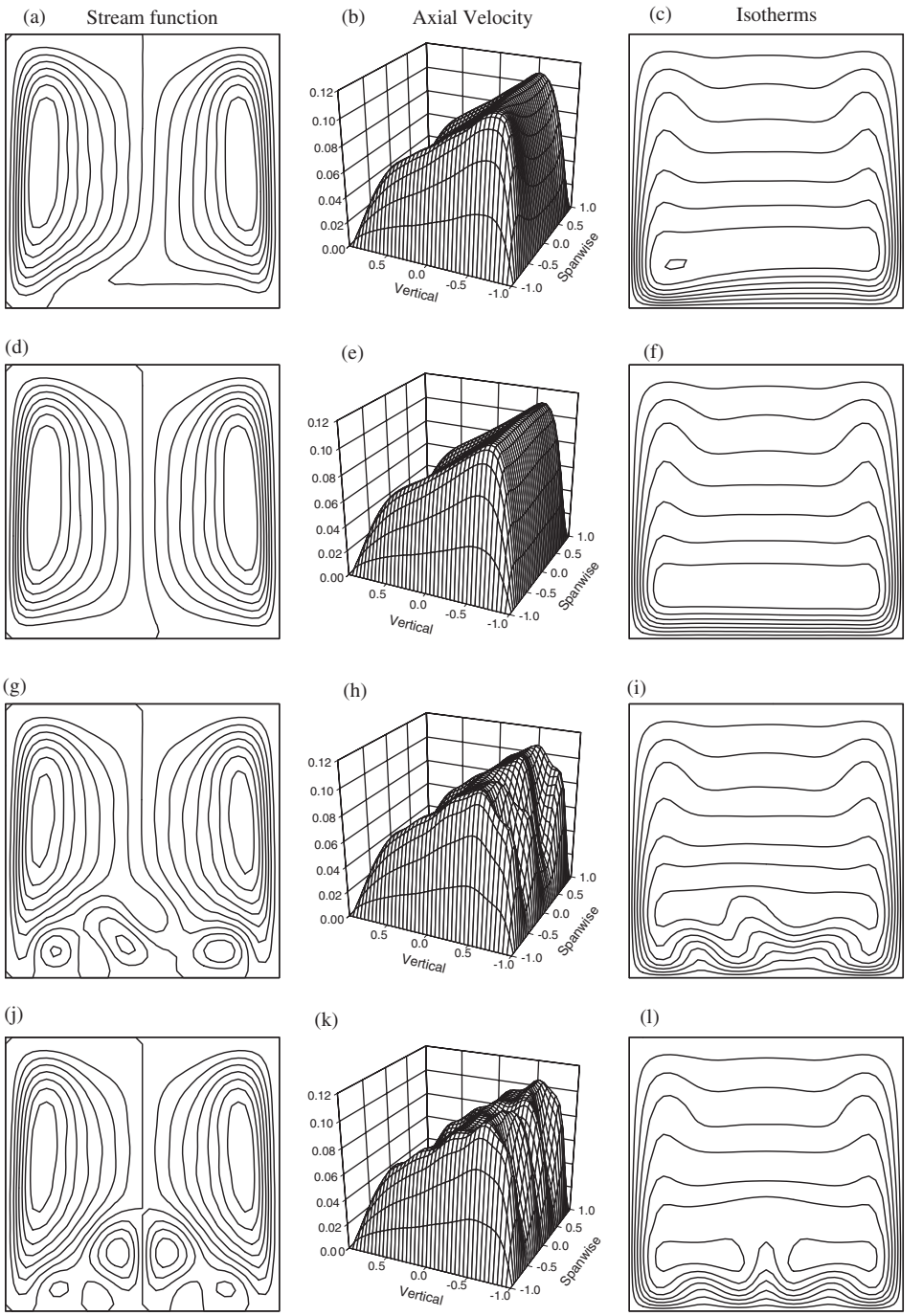

Figure 8. Contour plots for the stream function, axial velocity perspective plots, and isotherm contours for $\lambda = 1 \times 10^7$, $\gamma = 1$, $Pr = 0.73$, $\phi = 0^\circ$. (a–c) solution on AS2, (d–f) solution on AS3, (g–i) solution on AS4, (j–l) solution on S2 after L3.

Table IV. Summary of eigenvalue calculations for $\gamma = 1$, $Pr = 0.73$, $\phi = 0°$.

λ	Branch	Symmetric modes	Asymmetric modes
7×10^5	S1 (before L2)	Stable	Stable
	S1 (L1–L2)	9.870558	7.523110
	S1 (after L1)	Stable	13.132214
1.5×10^6	S1	Stable	17.627994
	AS1		$6.38 \pm 19.55i$
3×10^6	S2 (L4–L9)	Stable	Stable
	S2 (after L3)	89.582002	55.434788
			37.390757
	S1	Stable	23.673250
	AS2		$40.76 \pm 14.33i$
			$4.914 \pm 15.23i$
7×10^6	S1	Stable	32.683205
	S2 (L4–L9)	Stable	Stable
	S2 (L6–L9)	43.416402	46.042996
		$9.7881 \pm 39.953i$	$4.7605 \pm 41.938i$
	S2 (L6–L8)	$122.996 \pm 24.472i$	139.982345
			$60.909 \pm 31.797i$
	S2 (after L3)	144.568957	83.110162
			59.675914
	AS2		$81.0748 \pm 38.3719i$
			$51.2467 \pm 50.7445i$
1×10^7	S1	Stable	37.272314
			$14.1264 \pm 93.968i$
	S2 (after L7)	114.379112	$80.1593 \pm 37.826i$
		74.541829	68.669514
	S2 (after L3)	175.110949	104.447981
		$2.2509 \pm 144.758i$	69.305793
	AS2		$106.84086 \pm 55.006i$
			$79.23168 \pm 75.967i$
			$22.79704 \pm 63.368i$
	AS3		$14.126424 \pm 93.9681i$
	As4		168.902449
			106.971958
			93.407480
			$86.6159 \pm 61.840i$

SUMMARY AND CONCLUSIONS

We have presented two approaches on how to solve the governing equations of mixed-convection heat transfer through a horizontal duct by the spectral collocation method. It has been found that no advantage is gained in using the second approach over the first one. Six branches have been computed in the range of Grashof number between 0 and 2×10^6 for a Prandtl number of 0.73 and a duct of square cross-section without tilt. Nine limit points and five symmetry-breaking bifurcation points have been computed. We extended the range of Grashof number beyond what has been considered by Nandakumar and Weinitschke [8]. For the same range considered by Nandakumar and Weinitschke [8], the overall bifurcation structures found here and computed by them look similar. However, the stability properties of the computed branches disagree slightly with the results of Nandakumar and Weinitschke. In particular the two-cell flow structure on one end of the isolated branch is rather stable, while the four-cell flow on the other end is unstable. The two-cell flow of the main branch is also stable and the four-cell flow is only stable with respect to symmetric disturbances. All asymmetric branches develop unstable modes, but these modes are not as many as what has been reported by Nandakumar and Weinitschke. The computed limit points and symmetry-breaking points are in good agreement with the study of Nandakumar and Weinitschke for low Grashof numbers, but deviate slightly ($\sim$10% relative error) for high Grashof numbers.

NOMENCLATURE

ρ	density
ρ_r	density at a reference state
μ	absolute viscosity
v	kinematic viscosity
T'_r	temperature at a reference state
T'_w	wall temperature
T'_b	average bulk temperature
α	thermal diffusivity
β	coefficient of thermal expansion
$2a$	duct height
$2b$	duct width
γ	aspect ratio $(=b/a)$
ϕ	tilt angle
(x', y', z')	dimensional co-ordinates
p'	dimensional pressure
$\mathrm{d}p'/\mathrm{d}z'$	axial pressure gradient
$\mathrm{d}T'_b/\mathrm{d}z'$	average axial bulk temperature gradient
(u', v', w')	dimensional velocity components
T'	dimensional temperature
x	dimensionless x-co-ordinate $(=x'/b)$
y	dimensionless y-co-ordinate $(=y'/b)$
u	dimensionless x-velocity $(=u'/(v/a))$

v dimensionless y-velocity $(= v'/(v/b))$
w dimensionless z-velocity $(= w'/((-\mathrm{d}p'/\mathrm{d}z')(a^4/\rho v^2)))$
θ dimensionless temperature $(= T'_w - T')/[(\mathrm{d}T'_b/\mathrm{d}z')(-\mathrm{d}p'/\mathrm{d}z')(a^4/\rho v^2)])$
ψ stream function
Pr Prandtl number $(= v/\alpha)$
λ $(= (g\beta a^7/\rho v^4)(\mathrm{d}T'_b/\mathrm{d}z')(-\mathrm{d}p'/\mathrm{d}z'))$
N_x number of polynomials in the x-direction
N_y number of polynomials in the y-direction
$\langle w \rangle$ dimensionless average axial velocity
Re Reynolds number
f friction factor $(f\,Re = 8\gamma^2/[(1+\gamma)^2\langle w \rangle])$
$\langle \theta_b \rangle$ dimensionless average bulk temperature
Nu Nusselt number $(= 4\gamma^2\langle w \rangle Pr/((1+\gamma^2)\langle \theta_b \rangle))$

REFERENCES

1. Morton BR. Laminar convection in uniformly heated horizontal pipes at low Rayleigh numbers. *Quarterly Journal of Mechanics and Applied Maths* 1959; **12**:410–420.
2. Iqbal M, Stachiewics JW. Influence of tube orientation on combined free and forced laminar convection heat transfer. *Transactions of the ASME C: Journal of Heat Transfer* 1966; **88**:109–116.
3. Faris GN, Viscanta R. An analysis of combined forced and free convection heat transfer in a horizontal tube. *International Journal of Heat Mass Transfer* 1969; **12**:1295–1309.
4. Van Dyke M. Extended stokes series: laminar flow through a heated horizontal pipe. *Journal of Fluid Mechanics* 1990; **212**:289–308.
5. Cheng KC, Hwang GJ. Numerical solution for combined free and forced laminar convection in horizontal rectangular channels. *Transactions of the ASME C: Journal of Heat Transfer* 1969; **91**:59–66.
6. Patankar SV, Ramadhyani K, Sparrow EM. Effect of circumferentially nonuniform heating on laminar combined convection in a horizontal tube. *Transactions of the ASME C: Journal of Heat Transfer* 1978; **100**:63–70.
7. Chou FC, Hwang GJ. Combined free and forced laminar convection in horizontal rectangular channels for high Re–Ra. *Canadian Journal of Chemical Engineering* 1984; **62**:830–836.
8. Nandakumar K, Weinitschke HJ. A bifurcation study of mixed-convection heat transfer in horizontal ducts. *Journal of Fluid Mechanics* 1991; **231**:157–187.
9. Nandakumar K, Raszillier H, Durst F. Flow through rotating rectangular ducts. *Physics Fluids A* 1991; **3**: 770–781.
10. Selmi M, Nandakumar K, Finlay WH. A bifurcation study of viscous flow through a rotating curved duct. *Journal of Fluid Mechanics* 1994; **262**:353–375.

